npj | clean water

Article

Published in partnership with King Fahd University of Petroleum & Minerals

https://doi.org/10.1038/s41545-024-00347-0

A super-efficient gel adsorbent with over 1000 times the adsorption capacity of activated carbon

Menghan Hu[1,2], Na Xie[1,2], Yujia Huang[1] & Yikai Yu[1]

It was observed that a super-efficient gel adsorbent system (RRQG@CDC) could be obtained when a matrix material of polyquaternium gel with a flat distribution (RRQG) was loaded onto a skeleton material of cyclodextrin carbide (CDC). The results showed that the adsorption capacity of RRQG@CDC towards dyes was 1250 times higher than that of commonly used activated carbon, enabling highly efficient purification of dyeing wastewater through superior adsorption. In addition, RRQG@CDC demonstrated adaptability to a range of different pH values and salinity conditions, showing super-efficient adsorption abilities towards various types of dyes. Moreover, simulated scale-up tests confirmed the feasibility of this super-efficient adsorbent for practical engineering applications. An enhanced quasi-planar electrostatic adsorption mechanism model was established, which has changed the traditional understanding of adsorption mechanisms. Furthermore, the waste residues of RRQG@CDC, after dye adsorption, can be directly utilized as high-calorific fuels, showcasing the resourcefulness of these residues while eliminating the risk of secondary pollution. In conclusion, this study achieved a remarkably efficient and resource-based purification of dyeing wastewater by developing a highly effective adsorbent system.

Water is the source of human life, accounting for about 71% of the total surface area of the world. Water pollution has seriously threatened the environment on which human society depends[1–5]. Among them, dyeing wastewater with high chroma, high toxicity, and difficult biochemical degradation has become the main source of water pollution that destroys the ecological environment and is a key issue in water environment management[6,7]. The adsorption method is one of the most commonly used methods in water treatment to remove pollutants at low concentrations, thus increasing the water quality to meet the discharge standards[8–11]. Until now, activated carbon is still regarded as the most widely applied adsorbent in water treatment engineering. Activated carbon produces an efficient van der Waals force to adsorb the pollutants from water, a result of its porous structure and large specific surface area[12,13]. However, when adsorbing some pollutants with a high molecular volume, the use of activated carbon is often ineffective as the pore size is not large enough to accommodate the pollutants. For example, one of the author's previous studies showed that when a granular coal-based activated carbon was used for adsorbing dyes with a high molecular volume (Reactive Scarlet 3BS, its relative molecular mass is 1136.32 g mol^{-1}), the adsorption capacity was only 1.85 mg g^{-1} [14]. Therefore, the inability to adsorb pollutants with large molecular volumes is a major drawback of using activated carbon.

Considering the influence of interaction forces, the efficiency of adsorption correlates positively with the strength of the binding between the adsorbent and adsorbate. This effectiveness is determined by the types of interaction forces and the microstructures of the adsorbent[15–19]. In the author's subsequent studies, it was observed that the introduction of electrostatic adsorption could overcome the pore size limitation of activated carbon. Additionally, compared with the physical adsorptions based on van der Waals forces, the electrostatic adsorption (chemical adsorption) could form stronger chemical bonds between the adsorbent and adsorbate (e.g., anion–cation electrostatic ionic bonds), achieving efficient adsorption ability towards some pollutants with large molecular volumes[20–24]. The authors found that, based on the strong electrostatic structures of polyquaternium gel adsorbents, the adsorption capacity of dyes with large molecular volumes (Reactive Scarlet 3BS) increased by a factor of 741.10 compared to commonly used activated carbon. This was attributed to the strong electrostatic adsorption effect (i.e., ionic bonds)[25]. This research finding encouraged the authors to envision more effective performance improvements for polyquaternium gel adsorbents. The authors thought that if the adsorption

[1]School of Chemical Engineering, Jiangxi Normal University, Nanchang, China. [2]These authors contributed equally: Menghan Hu, Na Xie.
e-mail: yuyikai1980@163.com

capacity of polyquaternium gel adsorbents could be increased to over 1000 times higher than that of activated carbon, a major milestone in achieving the super-efficient purification of dyeing wastewater would be made. Nevertheless, such super-efficient adsorbent materials have not been reported so far.

The authors thought that the key to breaking through the performance limits of the existing polyquaternium gel adsorbents lies in overcoming the limits of the existing interaction mechanisms and the material skeleton functions[26–29]. According to the conventional understanding of the effect of skeleton spaces on adsorption, efficient adsorption usually occurs in the general three-dimensional adsorbent-skeleton spaces. For example, the adsorption of commonly used activated carbon occurs only within its porous three-dimensional skeleton space. Moreover, when a cationic gel adsorbent is placed in water, its structure expands because of water-soluble swelling. This forms a three-dimensional water-soluble swelling body that usually electrostatically adsorbs anionic pollutants (e.g., anionic dyes) in water in the form of a three-dimensional water-soluble swelling body. However, the efficiency of electrostatic adsorption at the cationic adsorption points on its surface and on its inside are different[30–32]. The cationic adsorption points on the surface of the gel have no contact obstacle with anionic dyes in water and can be directly and fully contacted, so relatively efficient electrostatic adsorption occurs[33–35]. Regarding the cationic adsorption points inside the gel, the anionic dyes in external water must penetrate into the internal space of the gel before effective mutual contact can occur[36,37]. However, the anionic dyes cannot easily penetrate into the gel because of the large molecular volumes. Therefore, the efficiency of electrostatic adsorption between the cationic adsorption points inside the gel and the anionic dyes was usually low. Therefore, the abilities of gel adsorbents distributed in the three-dimensional forms in the water phase were not fully utilized, limiting their adsorption capacity towards anionic dyes (Supplementary Fig. 1A). It is hypothesized that transforming the conventional three-dimensional distribution of cationic adsorption sites in existing gel adsorbents into a new nearly two-dimensional flat distribution could lead to enhanced exposure of these sites to water. This alteration could facilitate more efficient electrostatic adsorption interactions between the adsorbents and anionic dyes in water. Such a breakthrough has the potential to surpass the adsorption capacity limits of current gel adsorbents, thereby enabling more efficient purification of dyeing wastewater.

To achieve a more efficient method of purifying dyeing wastewater, the authors carried out a series of original research studies. Firstly, a type of polyquaternium gel with a flat distribution (i.e., the reactive hetero-ring-derived polyquaternium gel (RRQG)) was developed, which could be used as a matrix material for constructing the flat distribution of an adsorbent system. Subsequently, cyclodextrin carbide (CDC) was formed under solution carbonization conditions, serving as the carrier to accommodate the RRQG matrix material. This process reinforced the flat distribution of cation adsorption points. The RRQG matrix material was loaded onto the CDC carrier to form a super-efficient RRQG-loading-CDC adsorbent system (i.e., RRQG@CDC). This system exhibits an adsorption capacity that is 1250 times greater than that of activated carbon (Supplementary Fig. 2). In conjunction with these experimental studies, serial simulation experiments utilizing modern instrument analysis technologies were performed to analyze the interaction behaviors and evolution of the super-efficient adsorption process exhibited by the RRQG@CDC towards dyes. This culminated in the development of an enhanced quasi-planar electrostatic adsorption mechanism model that changed the traditional understandings of adsorption mechanisms. In addition, the functional characteristics of post-adsorption RRQG@CDC waste residues were studied to explore their potential for resource utilization. This approach aimed to demonstrate the resourcefulness of waste residues while mitigating the risk of secondary pollution from solid waste.

To summarize, this study revolutionized our understanding of the interaction mechanisms, surpassed the adsorption capacity limits of existing adsorbents to build a super-efficient adsorbent material system, and provided a new theoretical and technical basis for super-efficient and resource-based treatments for the purification of dyeing wastewater.

Results and discussion

Design, preparation, and functional characteristics of flat distributed matrix materials

The purpose of this study is to transform the conventional three-dimensional distribution of cationic adsorption points in existing gel adsorbents in water into a nearly two-dimensional flat distribution form. This alteration aims to overcome the limitations of existing adsorption mechanisms and achieve more efficient treatments of dyeing wastewater. A major problem lies in obtaining the matrix materials with a flat distribution in water. However, at present, there is no related research that could be directly referenced, so we could only solve this problem with an original design and experiments.

The authors' previous work showed that one similar material—a type of membrane polycarboxylate gel—could be obtained using a nitrogen-hetero-ring cationic monomer (*N*,*N*-diallyl-3-hydroxy-azacyclobutane ammonium chloride (DHAC)) and acrylic acid (AA) as the main reaction raw materials which go through the reaction processes of aqueous solution pre-copolymerization, baking, and ring-opening crosslinking (Supplementary Fig. 3A)[38]. Inspired by this previous work, the authors deduced that by following a similar preparation route and replacing the anionic acrylic acid (AA) with a cationic monomer (dimethyldiallylammonium chloride (DMDAC)), the RRQG would be obtained (Supplementary Fig. 3B). The membrane of the polycarboxylate gel appeared to display a form similar to that of a flat distribution. Given its structural similarity to RRQG, it can be inferred that RRQG may exhibit a flat distribution form

To obtain the optimized synthesis conditions, a four-factor three-level ($L_9(3)^4$) orthogonal experiment was designed. The effects of the reaction conditions—including monomer concentration (Factor *A*), reaction temperature (Factor *B*), initiator (APS) dosage (Factor *C*), and reaction time (Factor *D*)—on the synthesis of the RRQG material under different reaction temperatures were studied (see Supplementary Table 1). Using the dye removal ability of the obtained product as the evaluation index, the optimized synthetic reaction conditions for RRQG materials were determined as follows: a monomer concentration of 55%, a reaction temperature of 55 °C, an APS initiator dosage of 1%, and a reaction time of 6 h. Under these conditions, the RRQG material exhibited the highest dye removal percentage.

Under the optimized synthetic reaction conditions, the molar ratio of DHAC to DMDAC monomer in the reaction system was changed to control and regulate the structural composition of the RRQG product. The impact of these variations on the material's dye adsorption capacity from water is summarized in Supplementary Table 2. The results show that when the molar ratio of DHAC to DMDAC monomer was 10:90, the removal percentage of dyes was greatest, with a *R*% value of 99.66%. Therefore, this should be used as the target product for the optimized structural composition. Based on a scientific calculation, it was found that the cost of using this RRQG@CDC material should be lower than that of activated carbon, offering an additional incentive for its application (the detailed descriptions can be found in the "Supplementary Discussion: A calculation for cost for preparing RRQG@CDC material" section in "Supplementary Information," and the results are shown in Supplementary Table 3).

Through serial property exploration experiments, it was found that the obtained RRQG substance had flat distribution characteristics and achieved better adsorption ability when it was used as an adsorbent for purifying dyeing wastewater, as described below.

Directly observed by optical microscopy, the RRQG solid powder (as shown in Fig. 1A) immediately presented a planar annular distribution form when it was put into water (as shown in Fig. 1A—×100 magnification). This was a type of transitional form in which the RRQG substance diffused in the planar direction in the water phase, meaning that the RRQG substance had strong planar distribution characteristics in the water phase. Subsequently, with further diffusion and high penetration of the water, the annular distribution transition form disappeared and the RRQG substance dispersed into a transparent form (as shown in Fig. 1C—×100 magnification). Finally, after dye adsorption by the RRQG substance, the colored waste residues

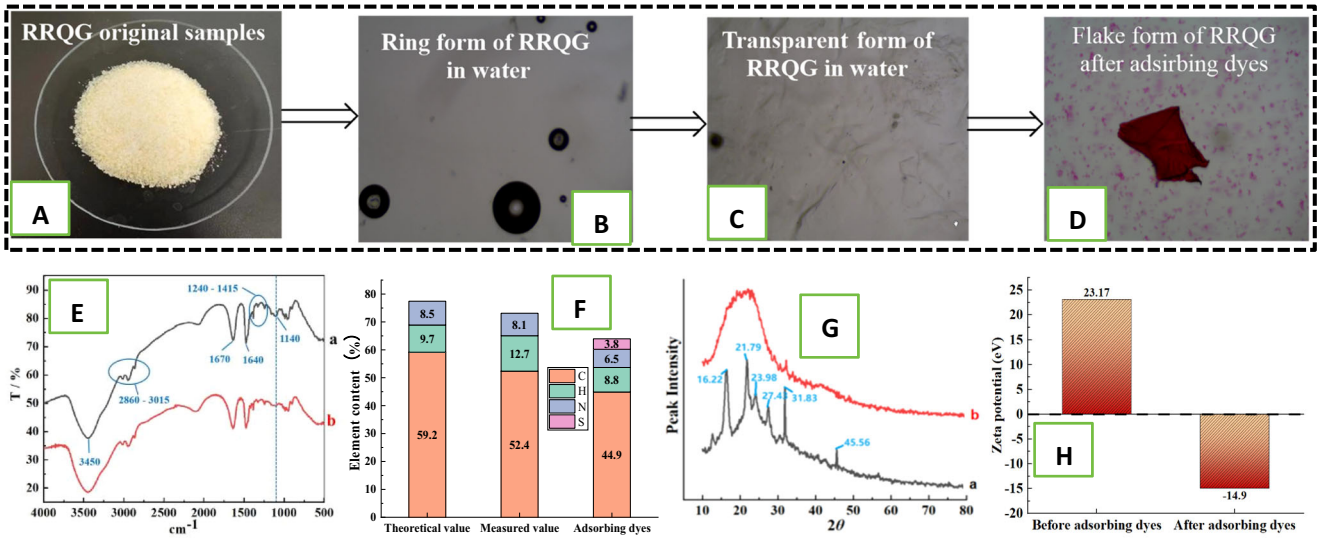

Fig. 1 | Microstructure transformations of RRQG before and after adsorbing dyes. A The photo for the RRQG original samples (magnification value: ×100). **B** The photo for ring form of RRQG in water (magnification value: ×100). **C** The photo for transparent form of RRQG in water (magnification value: ×100). **D** The photo for flake form of RRQG after adsorbing dyes. **E** Comparing the FT-IR analysis of RRQG before and after adsorbing dyes. **F** Comparing the theoretical value, measured value, and the value after adsorbing dyes for the element analysis of RRQG (with 10/90 of molar ratio of DHAC and DMDAC units). **G** Comparing the XRD analysis of RRQG before and after adsorbing dyes. **H** Comparing the zeta potentials of RRQG before and after adsorbing dyes (tested under pH value being 7).

appeared in a flat form (as shown in Fig. 1D—×100 magnification), which confirmed that the RRQG had the functional characteristics of a flat distribution form in the water phase.

The Fourier Transform infrared spectroscopy (FT-IR) spectra of the RRQG (Curve "a" in Fig. 1E) showed that there were absorption stretching vibration absorption peaks of an -OH group at 3450 cm^{-1}; a -C-H linkage at 2860–3015 cm^{-1}; bending vibration absorption peaks of an -N-H linkage at 1670 cm^{-1} and 1640 cm^{-1}; and in-plane bending vibration absorption peaks of a -C-H linkage at 1240–1415 cm^{-1}, which display a N-heterocyclic-derived polyquaternium-based structure. By contrast, the FT-IR spectra of the RRQG after dye adsorption (Curve "b" in Fig. 1E) showed an absorption peak outline similar to that of pure RRQG (Curve "a" in Fig. 1E). Additionally, the characteristic absorption peak intensity of -C-N linkages at 1140 cm^{-1} was slightly reduced, indicating that the RRQG maintained a relatively stable structural skeleton when adsorbing dyes. This is possibly caused by an efficient electrostatic interaction between the N-containing cations of the RRQG and the anionic dyes, leading to changes in the FT-IR absorption spectra.

The element analysis in Fig. 1F showed that the measured C, H, and N contents of the RRQG (DHAC to DMDAC molar ratio of 10:90) were 52.37%, 12.70%, and 8.06%, respectively. The corresponding theoretical values of these element concentrations were 59.16%, 9.74%, and 8.52%. Due to the uncontrollability and irregularity of the free radical copolymerization reaction between DHAC and DMDAC, there was a significant difference between the measured and theoretical C and H contents of the RRQG. However, the measured N content of the obtained RRQG (8.06%) was relatively close to the theoretical value (8.52%), indicating that the critical N-containing cationic moieties in the structure of obtained RRQG can be confirmed, as expected. These cationic moieties are the necessary foundation to generate an efficient electrostatic interaction between the RRQG and some anionic dyes.

The XRD analysis in Fig. 1G showed the changes in interior aggregation structures before and after RRQG adsorbed dyes. Before dyes were adsorbed by the RRQG, there were a number of sharp peaks at 16.22°, 21.79°, 23.98°, 27.43°, 31.83°, and 45.56° (Fig. 1G, Curve "a"), which correspond to some crystalline structures. However, after the dyes were adsorbed, the XRD analysis (Fig. 1G, Curve "b") only displayed a wide peak corresponding to an amorphous aggregation structure. This indicates that the crystal structures of the RRQG were significantly affected because of the doping effects of the adsorbed dyes. This phenomenon also indicated that the dyes had been fully adsorbed into the RRQG structures, thus completely changing the structure characteristics of the RRQG.

The zeta potential analysis in Fig. 1H shows that, before dyes were adsorbed, the RRQG displayed a strongly positively charged form, with the zeta potential equal to +23.17 eV. However, after dye adsorption, the zeta potential of the RRQG waste was −14.90 eV, corresponding to a strongly negatively charged form. This change is attributed to the extensive enrichment of anionic dyes into the RRQG structure, indicating efficient adsorption between the RRQG and anionic dyes.

Through isothermal adsorption experiments, the adsorption performance of RRQG materials towards dyes was studied, with the results shown in Fig. 2A. The RRQG dosage and dye removal percentage demonstrate a positive correlation, with a higher dosage of RRQG resulting in a greater dye removal percentage. This is in agreement with the general law relating the adsorbent dosage and the dye removal percentage. Generally speaking, the relationship between the amount of adsorbent and its equilibrium adsorption capacity (q_e) usually follows the law of diffusion in the presence of concentration gradients. In other words, when the amount of adsorbent is small, there is a large difference between the dye concentration inside and outside (in water) of the adsorbent. This concentration gradient results in a high driving force for diffusion, leading to the permeation of dyes in the water into a small amount of adsorbent space, achieving a stable concentration between the inside and outside of the adsorbent. Thus, equilibrium adsorption capacity is achieved (when the amount of adsorbent is small). However, when the dosage of the RRQG is less than 0.005 g, a larger RRQG dosage results in a greater equilibrium adsorption capacity, i.e., the dosage of the RRQG is directly proportional to its equilibrium adsorption capacity. This contradicts the conventional effects brought about by the concentration difference. This may be because when the RRQG dosage is larger, the greater the contacted surface area of cation interaction. When the dosage of the RRQG is greater than 0.005 g, the larger the dosage of the RRQG, the smaller the equilibrium adsorption capacity. This conforms to the conventional concentration difference diffusion law. If the maximum equilibrium adsorption capacity of the adsorbent is taken as its maximum adsorption capacity (Q_{max}), the maximum adsorption capacity of the RRQG for 100 mL of 100 mg L^{-1} Reactive Scarlet 3BS dye is calculated as 1881.59 mg g^{-1} when the dosage of RRQG is 0.005 g. This is a factor of 1017.08 greater than that of activated carbon and is also higher than similar

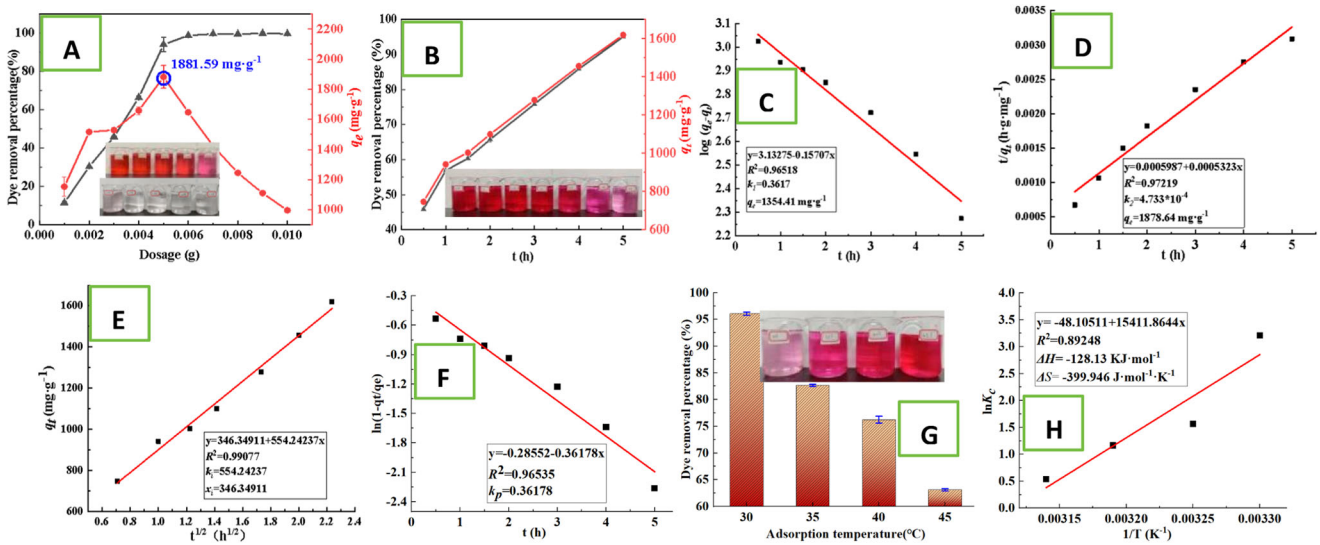

Fig. 2 | Isothermal, kinetics, and thermodynamics adsorption behaviors of RRQG towards dyes in water. A Isothermal adsorption results of RRQG towards dyes. **B** The adsorption results of RRQG towards dyes at different adsorption time. **C** Fitting the first kinetics model using the adsorption kinetics data. **D** Fitting the second kinetics model using the adsorption kinetics data. **E** Fitting the intra-particle diffusion model model using the adsorption kinetics data. **F** Fitting the particle diffusion model using the adsorption kinetics data. **G** The effect of different temperatures on RRQG treatment with dyes. **H** Fitting results of the thermodynamics model of RRQG treatment towards dyes.

adsorbent materials under the same conditions. Therefore, it can be said that RRQG materials with flat morphological distribution characteristics in water are more efficient at treating dyeing wastewater. This is a result of a superior adsorption capacity relative to existing gel adsorbents.

Based on multiple (six) parallel repeated experiments, the effects of different times (0.5–5.0 h) on the level of dye adsorption by the RRQG were systematically studied and its adsorption kinetics were evaluated. The results showed that for the same adsorption time, the differences in dye removal percentage (R%) between the repeated experiments were minimal, i.e., the experimental standard error was very small (see Fig. 2B). The process behaviors of dye adsorption by the RRQG are therefore extremely stable for a given time. Although there were several transitional forms (i.e., the ring form, transparent form, and flake form) occurring during the adsorption of dyes by the RRQG (Fig. 1C), these forms were only maintained for a small period of time and they disappeared within 0.5 h. Therefore, during the selected range of test time (0.5–5.0 h), the adsorption of dyes by the RRQG was extremely stable, i.e., the adsorption stability was not disturbed by the various forms of the RRQG.

The obtained adsorption data (the average values from the six times of repeated experiments) are used to fit the first-order kinetic model, the second-order kinetic model, the intra-particle diffusion model, and the liquid film diffusion model, with the results shown in Fig. 2C–F (The corresponding kinetic parameters were listed in Supplementary Table 1). The results showed that the correlation coefficient of the adsorption data best fits the intra-particle diffusion model, as demonstrated by the R^2 value of 0.99 (as shown in Fig. 2E). Therefore, this indicates that intra-particle diffusion adsorption is a fast-controlling step that affects the adsorption process of dyes by the RRQG. The equation $y = 554.24x + 346.35$ is fitted based on the intra-particle diffusion model, with its gradient providing the rate constant of the intra-particle diffusion model ($k_i = 554.24$ mg g^{-1} h$^{1/2}$). A larger value of k_i indicates that the internal diffusion rate of dye adsorption by the RRQG is accelerated, which may be related to the flat distribution form of the RRQG. On the one hand, it expands the diffusion area through which the dye permeates, while on the other hand it reduces the dye diffusion rate. Additionally, the intercept ($x_i = 346.35$) of the fitted intra-particle diffusion model indicates the diffusion rate when the concentration gradient is zero. Larger values of x_i indicate that the adsorption of dyes by the RRQG follows a process that is less affected by the concentration difference, and vice versa.

Based on multiple (six) parallel repeated experiments, the influence of temperature on dye adsorption is shown in Fig. 2G. At higher adsorption temperatures, the adsorption removal percentage (R%) of dyes by the RRQG decreases, indicating an exothermic reaction process. The relevant adsorption data (the average values from the six times of repeated experiments) are used to fit the Van't Hoff equation (Fig. 5H); the value of the correlation coefficient is 0.89 and the fitted equation is $y = 15{,}411.86x - 48.11$. By fitting the slope and intercept of the equation, the adsorption enthalpy change (ΔH) is calculated to be -128.13 kJ mol^{-1}, further indicating that the adsorption process is exothermic. The adsorption entropy change (ΔS) is calculated to be -399.95 J mol^{-1}, indicating that the disorder of the system is reduced after the dye is adsorbed by the RRQG (while the disorder of the substance system after conventional adsorption). Then, using the Gibbs free energy equation ($\Delta G = \Delta H - T\Delta S$) it is determined that $\Delta G < 0$ when the adsorption temperature is lower than 48.13 °C. This meets the condition of spontaneous adsorption. There is an upper temperature limit in the process of spontaneous adsorption of dyes by the RRQG, but there is no temperature limit in conventional exothermic adsorption. However, this condition could also meet the requirements of normal application. Therefore, the adsorption of dyes by the RRQG follows an unconventional adsorption thermodynamic process, demonstrating that the adsorption mode of the RRQG differs from conventional adsorbents.

Discovery and characteristics of CDC

Carbonized materials (such as activated carbon) are the most commonly used adsorbent materials in industry at present; however, they are usually obtained by carbonization at high temperatures (e.g., above 500 °C). Therefore, there are some drawbacks, such as harsh reaction conditions, difficulty in controlling the reaction process, and high requirements for equipment. In one exploratory experiment of CD modification, the authors found that a new black substance—CDC—was unexpectedly obtained after the CD hydrochloric acid solution was heated to 100 °C in an oven, evaporated, and dried (as shown in Fig. 3A–C). It was the first time carbonized materials were obtained by the simple solution carbonization process, overcoming the shortcomings of the traditional high temperature carbonization process.

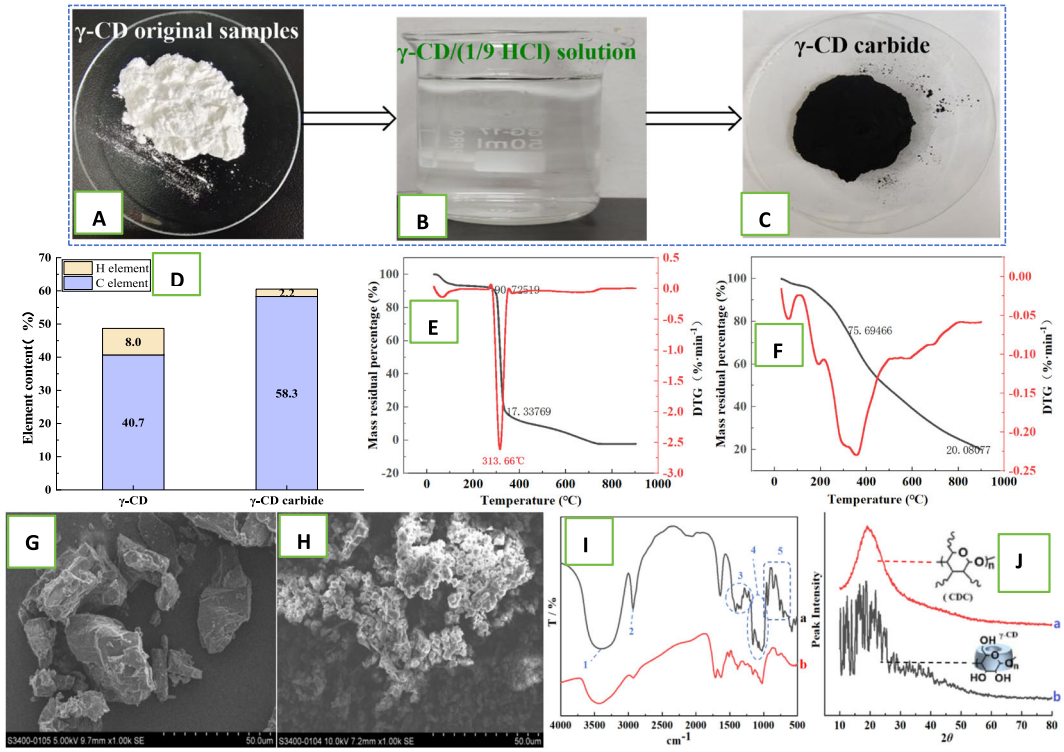

Fig. 3 | Formation process and microstructure transformations form CD to CDC. **A** The photo for the original γ-CD samples. **B** The photo for the γ-CD (1/9 HCl, v/v) solution. **C** The photo for the γ-CD carbide (CDC). **D** The element analysis of CD and CDC. **E** TG-DTG analysis of CD in N_2 atmosphere. **F** TG-DTG analysis of CDC in N_2 atmosphere. **G** SEM analysis of CD. **H** SEM analysis of CDC. **I** Comparing the FT-IR analysis of CD and CDC. **J** Comparing the XRD analysis of CD and CDC.

The dispersion (or solubility) of CDC in water and various organic solvents was observed by optical microscopy. The results show that, unlike pure CD which has a certain solubility in some solvents, CDC is dispersed in the form of particles, i.e., it is not dissolved. Therefore, CDC is neither soluble in water nor in various organic solvents (see "Supplementary Discussion: Dispersion (or solubility) of CDC in various solvents" section in "Supplementary Information," and the results are shown in Supplementary Fig. 4), indicating that it is a new substance with different characteristics to pure CD.

The elemental analysis in Fig. 3D shows that the content of C in the CDC samples is 58.39%, which is 43.53% higher than that of pure CD. This proves that CDC has a carbonized structure with a high carbon content. The content of H in the CDC samples is 2.23%, which is only 27.88% of that in pure CD samples. This may be because the carbonization of CD is caused by the elimination of hydroxyl groups in its structure.

Based on the thermogravimetric analysis, the behaviors of CDC and pure CD samples in an N_2 atmosphere were comparatively studied, with the results shown in Fig. 3E. Generally, the heat resistance of CDC was stronger than that of pure CD. In the N_2 atmosphere, the thermogravimetric process of pure CD simulates the basic law of high temperature carbonization. Firstly, a sharp thermal mass loss occurs at about 313.6 °C, while the residual percentage of the samples dropped sharply from 90.73% to 17.34%, which might be due to hydroxyl elimination (carbonization). Subsequently, with the rising temperature, the pure CDC was slowly degraded further. At the upper temperature limit of 900 °C, no residual mass was measured, indicating that the pure CD sample had almost completely decomposed (gasified). For CDC, slow thermal mass loss occurs in the temperature range of 100–900 °C. At the temperature corresponding to the sharp thermal mass loss of pure CD (313.66 °C), the residual percentage of CDC was as high as 75.69%. Even at the upper temperature limit of 900 °C, the residual percentage of CDC was still 20.08% (Fig. 3F). Therefore, it was inferred that CDC has a carbonized skeleton structure that is resistant to high temperatures and its heat resistance is greater than CD, providing further evidence that CDC could be used to obtain more effective carbonized materials.

Scanning electron microscopy (SEM) showed that pure CD was in the form of large dense particles (Fig. 3G). An explanation for this could be that the structure of pure CD contains a large number of hydroxyl groups and the hydrogen bonds generated by these groups are beneficial in regards to condensing the interior of the substance. Contrastingly, the CDC samples contained small, fragmented particles, as shown in Fig. 3H. This might be because of the elimination of a large number of hydroxyl groups in the carbonization process and the release of volatile substances (water), leading to a decrease in the internal cohesion of the substance and the development of a porous structure. It was further confirmed that the carbonization of CD might be caused by the elimination of hydroxyl groups in its structure.

The FT-IR spectra of pure CD (Curve "a" in Fig. 3I) shows a stretching vibration absorption peak of an -OH group at 3430 cm^{-1} (Peak 1); a stretching vibration absorption peak of a $-CH_2-$ linkage at 2930 cm^{-1} (Peak 2); the plane-bending vibration absorption peak of an -OH group at 1260–1467 cm^{-1} (Peak 3); the stretching vibration absorption peak of a C-O-C linkage at 1050 cm^{-1} (Peak 4); and the vibration absorption peak of the CD skeleton at 650–800 cm^{-1} (Peak 5), which displays a polyhydroxylated organism structure for pure CD. By contrast, the FT-IR spectra of CDC (Curve "b" in Fig. 3I) shows a weaker vibration absorption intensity of the -OH group at 3430 cm^{-1} (Peak 1 of Curve "a" in Fig. 3I), while still maintaining the absorption peaks corresponding to Peaks 2–5 of Curve "a" in Fig. 3I. This suggests that the carbonization of CD (to form CDC) is a process that involves the elimination of hydroxyl groups but maintains the basic molecular skeleton of CD.

The XRD analysis in Fig. 3J shows many intensive sharp peaks corresponding to crystalline aggregation structures in the pure CD sample (Curve "a" in Fig. 3J). However, in the CDC sample without carbonization, a wide peak corresponding to an amorphous aggregation structure is displayed in the XRD curve (Curve "b" in Fig. 3J). This might be due to the elimination of hydroxyl groups during the carbonization process of CD, weakening the directional hydrogen bonds between molecules and reducing

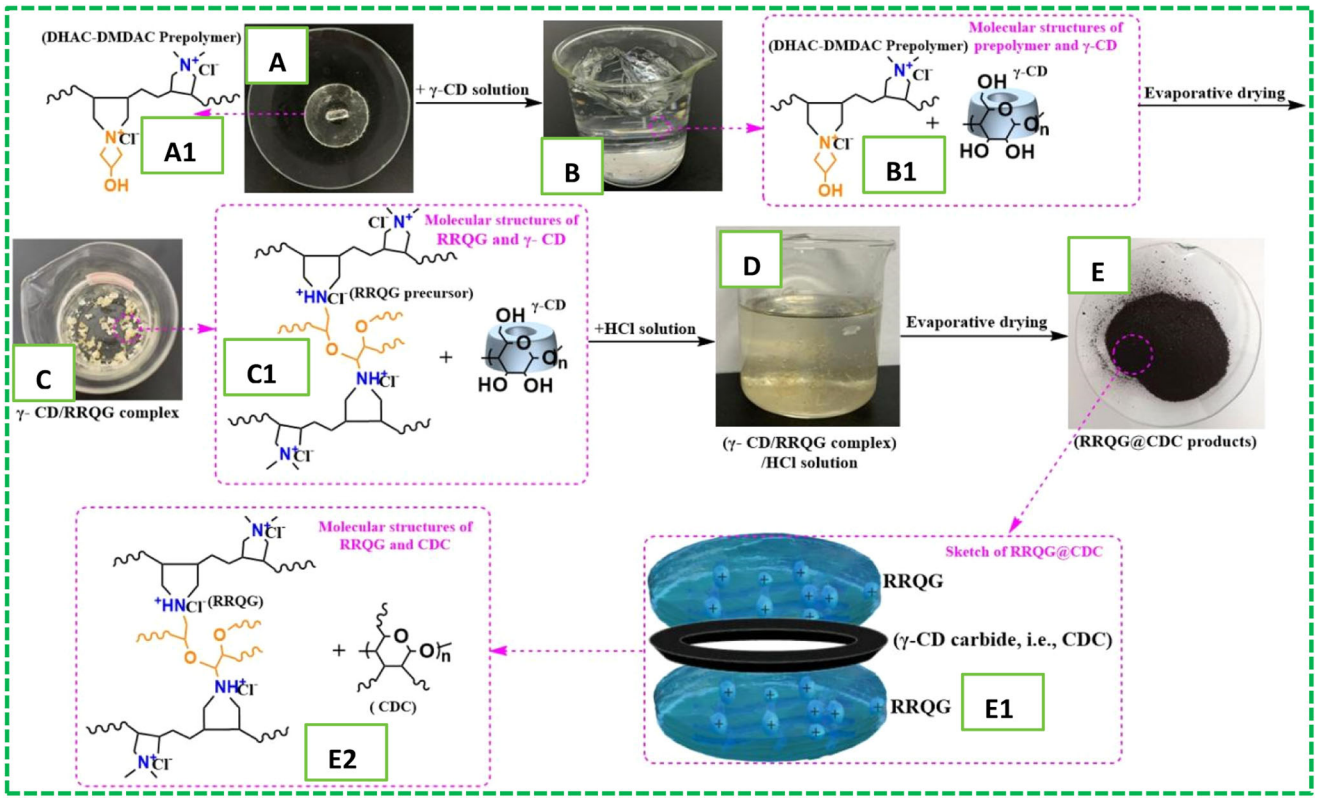

Fig. 4 | Schematic diagram for the formation process of RRQG@CDC adsorbent system. **A** The photo for the DHAC-DMDAC prepolymer. **A1** Molecular structure of DHAC-DMDAC prepolymer. **B** The photo for the DHAC-DMDAC prepolymer and γ-CD solution. **B1** Molecular structures of DHAC-DMDAC prepolymer and γ-CD. **C** The photo for the γ-CD/RRQG complex. **C1** Molecular structures of RRQG and γ-CD. **D** The photo for the (γ-CD/RRQG complex)/HCl solution. **E** The photo for the RRQG@CDC products. **E1** Model diagram of RRQG@CDC. **E2** Molecular structures of the RRQG@CDC-containing main compositions, i.e., RRQG and CDC.

the ordered arrangement of molecules. Overall, this results in an amorphous aggregation structure of CDC.

To summarize, the solution carbonization effect of CD may be caused by the elimination of hydroxyl groups in its structure, while the hydrogen bonds generated by the intramolecular hydroxyl groups result in the formation of the inner cavity ring structure. The elimination of hydroxyl groups leads to a weakening of intramolecular hydrogen bonds, resulting in the disintegration of the ring structure in the inner cavity of CD, thus forming CDC with a flatter distribution. As CDC may be a type of flat skeleton structure, it is similar to the flat distribution of the RRQG matrix materials. Furthermore, it is assumed that the RRQG-loaded CDC adsorbent material system (RRQG@CDC) can be obtained if the RRQG matrix materials with a flat distribution are loaded onto the CDC skeleton and the planar distribution of the RRQG cation adsorption points are consolidated with CDC as the carrier. The RRQG@CDC system has better water purification performance characteristics relative to conventional adsorbents; therefore, the potential of this material should be investigated further.

Construction, structural evolution, and functional characteristics of the super-efficient RRQG@CDC adsorbent system

As designed, the advantages of the RRQG and CDC are complementary; the flat distribution of the RRQG cation adsorption points consolidate with CDC as the carrier, obtaining an adsorbent RRQG@CDC material system with superior performance relative to conventional adsorbents. The preparation process is shown in Fig. 8. Firstly, 2.0 g of the DHAC-DMDAC prepolymer (Fig. 4A, A1) was soaked in 100 mL of 1% (w/w) γ-CD solution (Fig. 4B, B1) and the two were fully mixed and soaked. After evaporating and drying at 100 °C, the DHAC-DMDAC prepolymer formed the RRQG in situ in the γ-CD solution to obtain a γ-CD/RRQG complex (Fig. 4C, C1). Subsequently, the γ-CD/RRQG complex was put into a hydrochloric acid solution for an acidification treatment for a certain period of time and then evaporated and dried at 100 °C. The complex contained within the γ-CD solution (Fig. 4D) was carbonized in a hydrochloric acid solution, with CDC forming in situ and subsequently loaded with the RRQG material to produce the RRQG@CDC adsorbent material system (Fig. 4E, E1, E2).

To obtain the optimal preparation conditions, the key variables in the preparation of RRQG@CDC adsorbent materials are as follows: the mass fraction of γ-CD in the solution during the acidification treatment (Factor *A*); the concentration of hydrochloric acid, i.e., the dilution ratio of the concentrated hydrochloric acid solution to H_2O (Factor *B*); the soaking reaction time of the γ-CD prepolymer (Factor *C*); the soaking reaction temperature (Factor *D*); the acidification treatment time (Factor *E*); and the acidification treatment temperature of the γ-CD/RRQG complex in the hydrochloric acid solution (Factor *F*). A six-factor three-level orthogonal experiment (i.e., an $L_{18}(3)^6$ orthogonal experiment) was designed to investigate the influence of these parameters on the preparation of the RRQG@CDC, as shown in Supplementary Table 4. When taking the adsorption ability of the obtained RRQG@CDC product as the evaluation index, the ideal parameters are as follows: a mass fraction of γ-CD in the acidification solution of 1% (which corresponds to a mass ratio of γ-CD/RRQG of 1:2); a concentration of the HCl solution of 1:9; a soaking time of 3 h; a soaking temperature of 60 °C; an acidification time of 2 h; and an acidification temperature of 40 °C. The corresponding RRQG@CDC product achieved the highest dye removal percentage with an *R*% value of 96.99%. These parameter conditions can therefore be considered optimal when preparing the RRQG@CDC.

The structural evolution of the RRQG@CDC during the formation process was analyzed by FT-IR, elemental analysis, and SEM. These results are discussed in the proceeding paragraphs.

By comparing the FT-IR curves of the RRQG (Curve "a" in Fig. 5A) and the RRQG@CDC (Curve "b" in Fig. 5A), the molecular structural

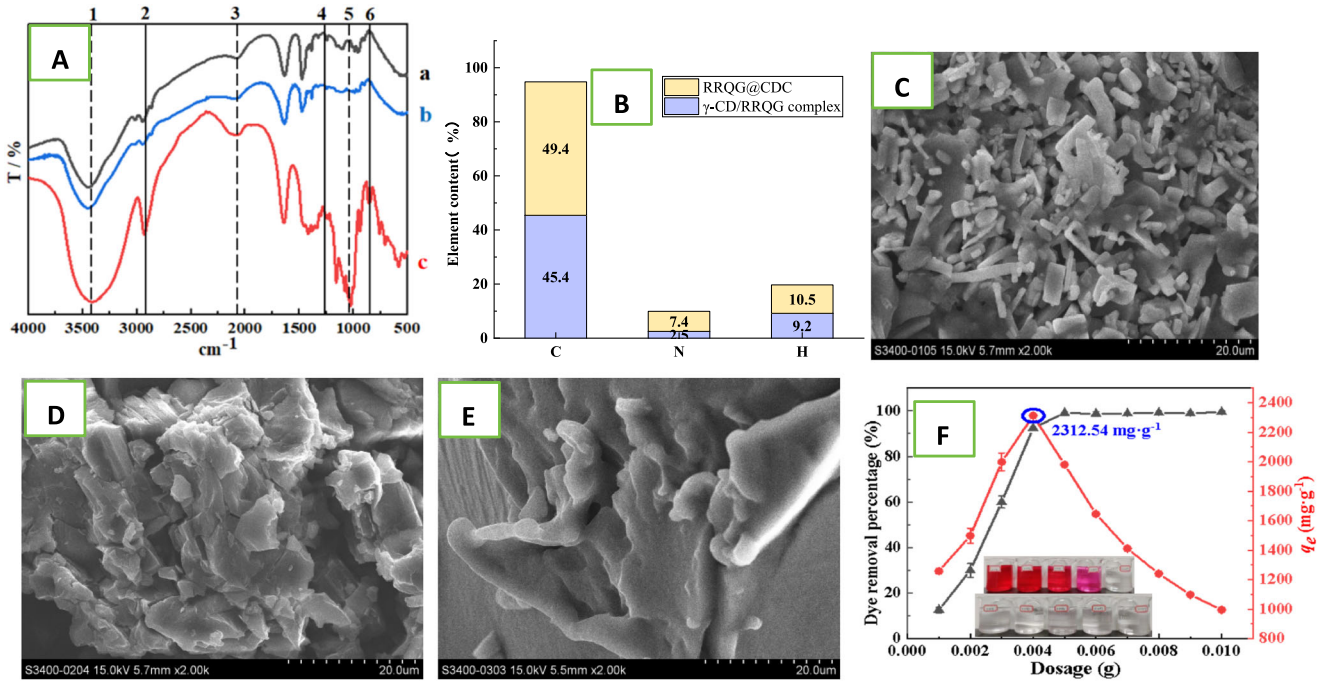

Fig. 5 | Microstructure transformations of RRQG@CDC formations and isothermal adsorption results of RRQG@CDC towards dyes. A Comparison of FT-IR analysis: (a) RRQG matrix (this is only for a comparison sample); (b) RRQG@CDC product; (c) γ-CD/RRQG complex without acidification (this is only for a comparison sample). **B** Comparing the element analysis of γ-CD /RRQG complex and RRQG@CDC. **C** SEM analysis of RRQG matrix (this is only for a comparison sample). **D** SEM analysis of γ-CD/RRQG complex without acidification (this is only for a comparison sample). **E** SEM analysis of RRQG@CDC product. **F** Adsorption ability analysis for RRQG@CDC product to treat the dyeing wastewater (a dye solution of Reactive Scarlet 3BS).

evolution during the formation of the γ-CD-modified RRQG can be studied. The two substances displayed similar trends, indicating that γ-CD containing a large amount of -OH is introduced during the formation process of the γ-CD-modified RRQG; however, the -OH group is subsequently eliminated in a specific process (e.g., acidification treatment). From Fig. 5A, comparing Curve "c" (sample of the γ-CD/RRQG complex without acidification) with Curve "b" (sample of the RRQG@CDC) reveals information about the molecular bonds present at each stage of the formation process. Curve "c" shows that the intramolecular hydrogen bonds at 3450 cm^{-1} (Peak 1 in Fig. 5A) and the absorption peak of primary alcohol at 1050 cm^{-1} (Peak 5 in Fig. 8A) were obviously weakened. Comparing the infrared curves of the RRQG (Curve "a" in Fig. 8A), the RRQG@CDC (Curve "b" in Fig. 5A), and the γ-CD/RRQG complex without acidification (Curve "c" in Fig. 5A) shows an increase in intensity, followed by a decrease, of the following peaks: absorption peak of telescopic vibration at 2950 cm^{-1} (Peak 2 in Fig. 5A); conjugate bonds at 2100 cm^{-1} (Peak 3 in Fig. 5A); C-H in-plane bending vibration at 1250 cm^{-1} (Peak 4 in Fig. 5A); and out-of-plane bending vibration of olefins at 850 cm^{-1} (Peak 6 in Fig. 5A). It is thus evidenced that there are structural changes during the reaction of the RRQG with modified γ-CD, with many C-H and C-C structures added after introducing γ-CD. Following the acidification treatment, the number of C-H and C-C structures is reduced.

The results of elemental analysis (Fig. 5B) showed that the contents of C, H, and N in the RRQG@CDC were higher compared to the γ-CD/RRQG complex without acidification treatment. This may be due to the elimination of -OH in γ-CD during acidification and carbonization, resulting in an increase of C, H, and N.

The SEM analysis shows that the structure of the dried RRQG samples is loose and irregular (Fig. 5C). The structure of the γ-CD/RRQG complex without acidification is relatively condense; however, the surface is still rough (Fig. 5D), which may be due to the effective adhesion action between γ-CD and the RRQG. Contrastingly, the surface of the RRQG@CDC is smoother (Fig. 5E), which may be attributed to the elimination reaction of -OH in γ-CD during acidification and carbonization, leading to a "flattening" effect on the surface of this substance.

In addition, the adsorption performance of the RRQG@CDC towards a dye of Reactive Scarlet 3BS was studied by multiple (six) parallel repeated experiments, with the results shown in Fig. 5F. The best removal percentage of the RRQG@CDC towards this dye was 99.60%. Meanwhile, similar to the previous RRQG, the RRQG@CDC did not follow the conventional law of diffusion in the presence of concentration gradients. Furthermore, its equilibrium adsorption capacity first increased and then decreased with an increase in its dosage. When the dosage of the RRQG@CDC was 0.004 g, the equilibrium adsorption capacity reached a maximum value of 2312.54 mg g^{-1}, which was regarded as the maximum adsorption capacity of the RRQG@CDC towards this dye.

Although there are many studies on adsorbents reported in the current literature, only the adsorption results under equivalent adsorption conditions are comparable. To objectively compare the adsorption superiority of RRQG@CDC to existing adsorbents, the authors selected the reported adsorption results of some existing adsorbents towards the Reactive Scarlet 3BS dye, with the findings summarized in Supplementary Table 5. Compared with the previous RRQG adsorbent materials, the Q_{max} of the RRQG@CDC increased by 430.95 mg g^{-1}, which showed that the dye adsorption capacity of adsorbent materials had been successfully improved by loading the RRQG into a CDC skeleton. Additionally, the Q_{max} of the RRQG@CDC was much higher than the similar adsorbent materials reported earlier, particularly compared to the commonly used activated carbon, where an increase by a factor of 1250 is observed. Once again, this demonstrates the super-efficient adsorption ability of the RRQG@CDC, highlighting its suitability for purifying dyeing wastewater.

To investigate the universality and applicability of the RRQG@CDC in the treatment of dyeing wastewater, its extended application under different conditions was studied, with the results shown in Fig. 6. When the pH is ≤7, the removal percentage of dyes treated by the RRQG@CDC (99.14–99.71%) was significantly higher than that under alkaline conditions, i.e. a pH >7

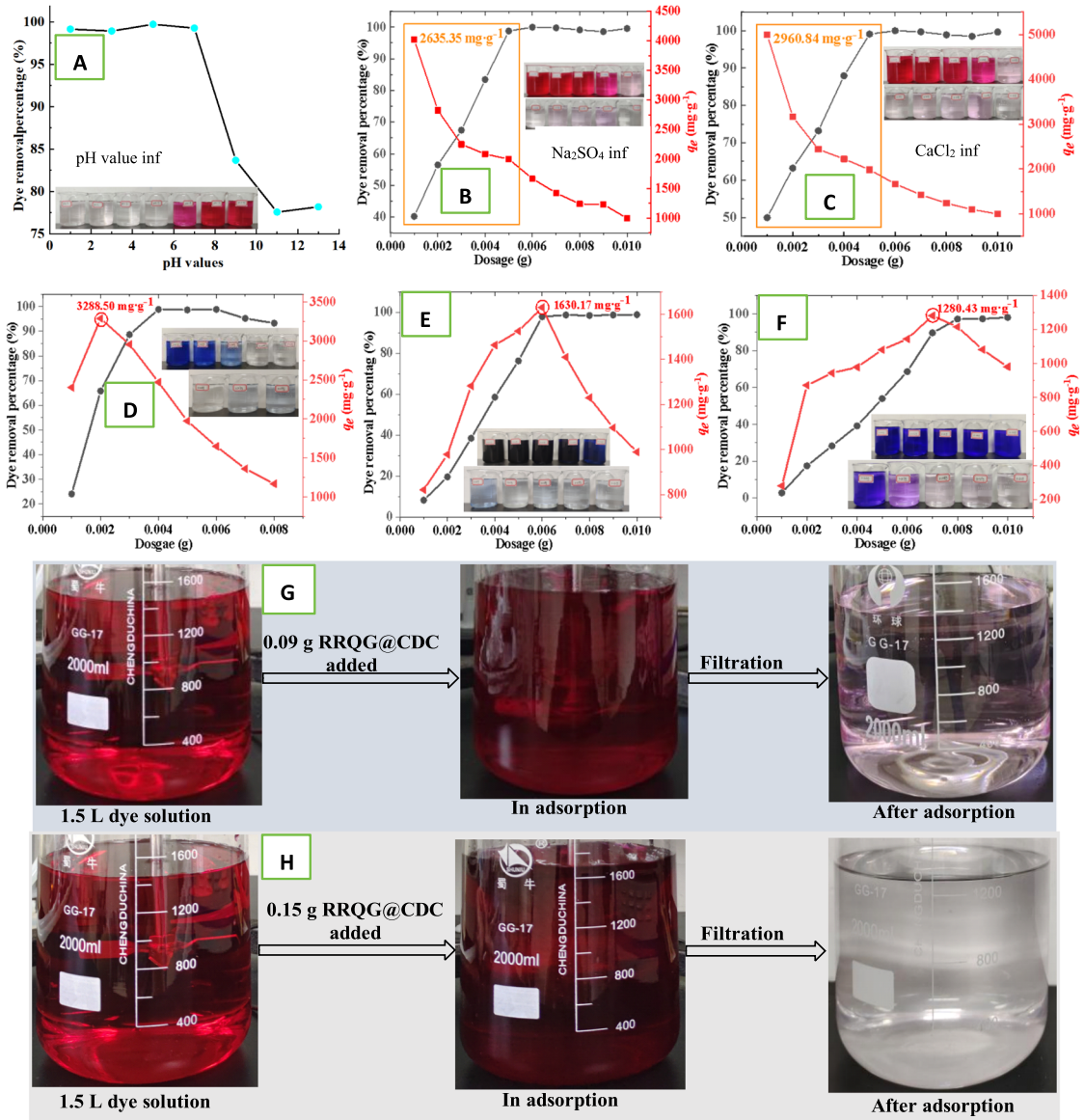

Fig. 6 | The universality and applicability of RRQG@CDC in treatment of dyeing wastewater. A Effect of different pH values on the adsorption of RRQG@CDC towards the dyes (Reactive Scarlet 3BS). **B** Effect of Na_2SO_4 presence on the adsorption of RRQG@CDC towards the dyes (Reactive Scarlet 3BS). **C** Effect of $CaCl_2$ presence on the adsorption of RRQG@CDC towards the dyes (Reactive Scarlet 3BS). **D** Adsorption ability analysis for RRQG@CDC towards the dye solution of Reactive Blue 19. **E** Adsorption ability analysis for RRQG@CDC towards the dye solution of Reactive Black KN-B. **F** Adsorption ability analysis for RRQG@CDC towards the dye solution of Methyl Blue. **G** A simulation scale-up application of 0.09 g RRQG@CDC used to treat a 1.5 L 100 mg L^{-1} dye solution of Reactive Scarlet 3BS. **H** A simulation scale-up application of 0.09 g RRQG@CDC used to treat a 0.15 L 100 mg L^{-1} dye solution of Reactive Scarlet 3BS.

(78.18–83.67%). This indicates that the RRQG@CDC is suitable for neutral or acidic conditions, as shown in Fig. 6A.

Under a certain salinity, such as 0.5% (w/w) of Na_2SO_4 or $CaCl_2$ (in which the total ionic concentrations could be respectively measured as 0.038 mol L^{-1} and 0.045 mol L^{-1} by ion chromatography technology), the RRQG@CDC still maintained a strong dye adsorption capacity. For example, when the dosages were above 0.005 g, the dye removal percentages were 98.57–100%. However, interestingly, the existence of salts in water changed the relationship between the dosage of the RRQG@CDC and the equilibrium adsorption capacity. In the case of Na_2SO_4 or $CaCl_2$, with an increased dosage of the RRQG@CDC, the equilibrium adsorption capacity of the RRQG@CDC decreased, following the conventional concentration gradient diffusion law (as shown in Fig. 6B, C). However, when the RRQG@CDC adsorbed dyes without salt, it did not follow the law of concentration gradient diffusion (see the previous Fig. 5F). This could be because the existence of salt substances reduces the equilibrium solubility of dyes in water, thus promoting the transfer of dyes from the water phase to the adsorbent phase, generating an additional effect similar to diffusion in the presence of concentration gradients. According to general rules, based on the average of the equilibrium adsorption capacity of the RRQG@CDC towards dyes in a saturated adsorption state (when the dosage of the RRQG@CDC was 0.001–0.005 g), the maximum adsorption capacity (Q_{max}) of the RRQG@CDC towards dyes under salt-containing conditions was calculated to be 2635.35 mg g^{-1} for Na_2SO_4 presence and 2960.84 mg g^{-1} for $CaCl_2$ presence, which were slightly higher than the Q_{max} value (2312.54 mg g^{-1}) from the experiment without any additional ions. Through the ion chromatography technology, it was observed that the remaining total ion concentrations after adsorptions in Na_2SO_4 (0.5%, w/w), $CaCl_2$ (0.5%, w/w), and the salt-free solutions were 0.1049 mol L^{-1}, 0.0786 mol L^{-1}, and 0.0355 mol L^{-1}, respectively, which were clearly higher than those of original solutions before adsorptions, possibly because an efficient ion exchange interaction occurred in the electrostatic adsorption of

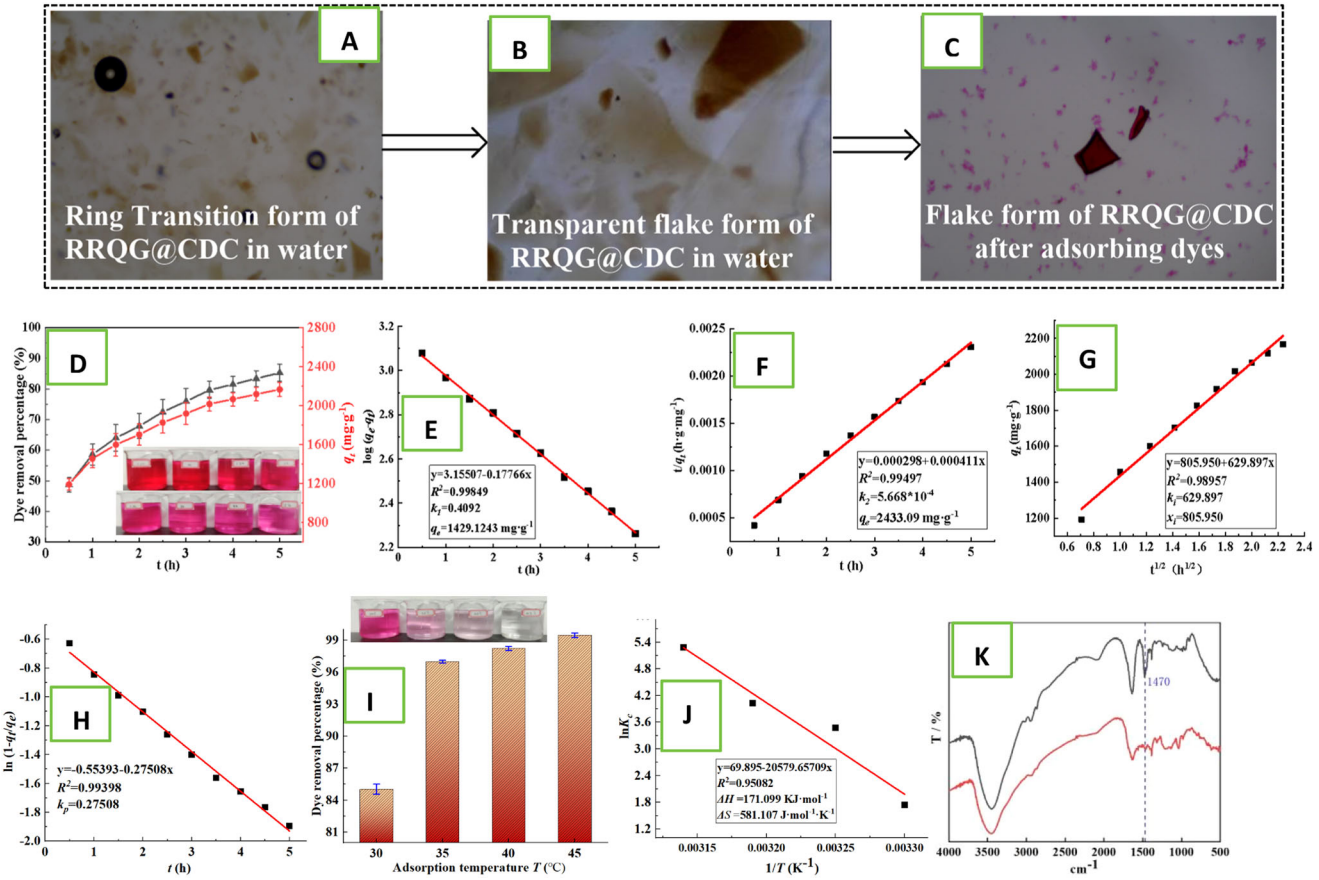

Fig. 7 | Optical microscope observations, kinetics adsorption behaviors, thermodynamics adsorption behaviors, and FT-IR analysis for RRQG@CDC to adsorb dyes. A Optical microscope observation for the ring transition form of RRQG@CDC in water (magnification value: ×100). **B** Optical microscope observation for the transparent flake form of RRQG@CDC in water (magnification value: ×100). **C** Optical microscope observation for the flake form of RRQG@CDC after adsorbing dyes (magnification value: ×100). **D** The adsorption results of RRQG@CDC towards dyes at different adsorption time with multiple parallel repeated experiments (six times). **E** Fitting the first kinetics model using the adsorption kinetics data. **F** Fitting the second kinetics model using the adsorption kinetics data. **G** Fitting the intra-particle diffusion model model using the adsorption kinetics data. **H** Fitting the particle diffusion model using the adsorption kinetics data. **I** The effect of different temperatures on RRQG@CDC treatment with dyes. **J** Fitting results of the thermodynamics model of RRQG@CDC treatment towards dyes. **K** Comparing the FT-IR analysis of RRQG@CDC before and after adsorbing dyes.

RRQG@CDC towards dyes, so as to additionally increase more salt substances in water.

When the RRQG@CDC was used to adsorb other dyes, such as Reactive Blue 19, Reactive Black KN-B, and Methyl Blue, the best dye removal percentages were 98.04–98.84%. The corresponding adsorption capacities of the RRQG@CDC reached 3288.5, 1630.17, and 1280.43 mg g^{-1} (Fig. 6D–F), respectively. The RRQG@CDC shows superior adsorption capacities for all of these dyes; therefore, it has a wide range of universality and applicability in the super-efficient treatment of dyeing wastewater.

To carry out several simulated scale-up tests of water treatment applications, the adsorption conditions shown in the previous Fig. 8F were used as a guide, with the amount of dye solution to be treated increased by a factor of 15 up to 1.5 L and the other application parameters changed proportionally (Fig. 6G–H). Figure 6G shows the results of a scale-up test using 0.09 g of the RRQG@CDC to treat a 1.5 L 100 mg L^{-1} dye solution of Reactive Scarlet 3BS. A dye removal percentage of 98.57% was achieved, which is near to the value (98.13%) of small-scale experiments under the same conditions when 0.006 g of the RRQG@CDC was used to treat 100 mL of the same dye (see the previous Fig. 5F). Meanwhile, Fig. 9H shows results when using 0.15 g of the RRQG@CDC to treat a 1.5 L 100 mg L^{-1} dye solution of Reactive Scarlet 3BS. A dye removal percentage of 99.15% was achieved (the water had fully become clean), which was also near to the value (99.83%) of small-scale experiments under equal conditions when 0.01 g of the RRQG@CDC was used to treat 100 mL of the same dye (see the previous Fig. 5F). Therefore, the RRQG@CDC demonstrates good scale-up ability for practical engineering applications.

Considering that the RRQG@CDC was suitable for an interaction model with a fixed solid-to-liquid ratio (similar to the coagulant's coagulation interaction model), the RRQG@CDC material could be added at the coagulation stage in a possible practical wastewater treatment. After complete interactions, the resulting sediment waste would be collected for resourcefulness [The detailed descriptions can be seen in the "Supplementary Discussion: The possible application of RRQG@CDC in practical wastewater treatment" section in "Supplementary Information," and the schematic diagram can be seen in Supplementary Fig. 5].

The super-efficient adsorption interaction mechanism of the RRQG@CDC towards dyes

Through serial simulation experiments and several modern instrument analysis technologies (e.g., optical microscopy, FT-IR, SEM-EDS, XRD, X-ray photoelectron spectroscopy (XPS), and zeta potential analysis), the interaction mechanisms between the RRQG@CDC and dyes were thoroughly explored.

The apparent morphological changes of the RRQG@CDC in water were directly observed by optical microscopy, with the RRQG@CDC displaying a similar morphology to the previous RRQG in water. At first, the RRQG@CDC shows an annular transition form (as shown in Fig. 7A —×100 magnification). Subsequently, with an increasing diffusion depth

and the high penetration of water, the RRQG@CDC dispersed from the annular distribution form to the transparent form (as shown in Fig. 7B—×100 magnification). After fully adsorbing the dyes, the RRQG@CDC waste residue takes on a flakey form in water (as shown in Fig. 7C—×100 magnification), which is similar to the previous RRQG.

According to the experiment methods in Section S9 in "Supplementary Information", the water swelling percentage (SP%) of RRQG@CDC could be measured as 5680%, i.e., the RRQG@CDC adsorbed 56.80 times its mass of water. This means that the RRQG@CDC has good water permeability in water, which is beneficial for the RRQG@CDC to fully contact with dyes, thereby effectively adsorbing the dyes in water.

Based on multiple (six) parallel repeated experiments, the effects of different times (0.5–5.0 h) on the level of dye adsorption by the RRQG@CDC were systematically studied, with the results shown in Fig. 7D. When comparing at the same adsorption time (t), the dye removal percentages (R%) obtained by different repeated experiments were vastly different (i.e., the experimental standard error was large). This observation demonstrates a changeable adsorption state during this adsorption time range, which is very different from the stable adsorption state of the RRQG towards the dyes during the same adsorption time range (see the previous Fig. 2B). This is possibly because the stabilization after forming the RRQG@CDC made it maintain transitional forms for a longer period of time compared to the RRQG. The various form transformations (from a ring form to a transparent form, and then to a flake form) of the RRQG@CDC could occur during this adsorption time range (0.5–5.0 h) so that the changeable (active) adsorption states of the RRQG towards the dyes could be observed. Regarding the adsorption capacity at different adsorption time, q_t reached 2167.67 mg g^{-1} when the adsorption time was 5.0 h, which was near the equilibrium adsorption capacity of 2312.54 mg g^{-1} at a time of 48 h (see the previous Fig. 5F). This indicates that most of the dye adsorption by the RRQG@CDC was achieved during the changeable adsorption stage.

Based on the average of repeated experimental data, the first-order kinetic model, second-order kinetic model, intra-particle diffusion model, and liquid film diffusion model were fitted to evaluate the dynamic trend of the RRQG@CDC adsorption towards dyes, with the results shown in Fig. 7E–H, respectively. The corresponding kinetic parameters are listed in Supplementary Tables 6 and 7 "Supplementary Information." The adsorption process of RRQG@CDC towards dyes conformed to the first-order kinetic model, the second-order kinetic model, the liquid film diffusion model, and the intra-particle diffusion model (all the correlation coefficients were above 0.99, as shown in Fig. 7E–H). Therefore, the adsorption of the RRQG@CDC towards dyes follows diversified adsorption models. The equilibrium adsorption capacity varied between the models. It took values of 1429.12 mg g^{-1} in the first-order kinetic model (Figs. 10E) and 2433.09 mg g^{-1} in the second-order kinetic model (Fig. 7F). This latter value is slightly higher than the q_e value (2312.54 mg g^{-1}) of isothermal adsorption shown in Fig. 9F, indicating that the second-order kinetic adsorption model best describes the adsorption capacity of the RRQG@CDC towards dyes.

The fitted equation of the intra-particle diffusion model of dyes adsorbed by the RRQG@CDC is $y = 629.89x + 805.95$ (Fig. 7G). Its slope value (k_i) is 629.89 mg g^{-1} $h^{1/2}$ and intercept value (x_i) is 805.95 were higher than the previous RRQG, indicating that the diffusion rate of dyes adsorbed by the RRQG@CDC was higher than that of the RRQG. This might be because the flat distribution of the RRQG cation adsorption points could be consolidated after it was loaded into CDC (forming RRQG@CDC). This process could be beneficial in achieving more efficient electrostatic interactions towards anionic dyes.

The effect of different temperatures on the adsorption characteristics of the RRQG@CDC towards dyes is shown in Fig. 7I. It can be seen that with the increase of adsorption temperature, the dye removal percentage increases, indicating that the adsorption process of the RRQG@CDC is an endothermic reaction. Contrastingly, the adsorption process of the RRQG is an exothermic reaction (see the previous Fig. 2F). This may be because the RRQG has a stronger consolidation effect on the CDC carrier skeleton, so it requires an endothermic reaction to stimulate and activate the adsorption reaction. The relevant adsorption data are used to fit the Van't Hoff equation (Fig. 7J), resulting in a correlation coefficient of 0.95 and a fitting equation of $y = -5981.3167x + 21.3446$. By fitting the slope and intercept of the equation, the adsorption enthalpy change (ΔH) is given as 171.09 kJ mol^{-1} and the adsorption entropy change (ΔS) is 581.11 J mol^{-1}. Then, using the Gibbs free energy equation ($\Delta G = \Delta H - T\Delta S$) it is determined that $\Delta G \leq 0$ when the adsorption temperature is lower than 21.42 °C and the adsorption of dyes adsorbed by the RRQG@CDC was spontaneous. This is the critical temperature for the RRQG@CDC to spontaneously adsorb dyes and is suitable for normal application requirements.

Through FT-IR analysis, the molecular structural changes of RRQG@CDC samples before and after dye adsorption were compared and analyzed, with the results shown in Fig. 7K. The characteristic absorption peak of the C-N^+ unit of the RRQG@CDC samples after adsorbing dyes (Curve "b" in Fig. 7K) is obviously weakened at 1470 cm^{-1} compared with the samples before dye adsorption (Curve "a" in Fig. 7K). This may be due to the effective electrostatic adsorption between the RRQG@CDC and dyes which blocks the C-N^+ characteristic unit.

SEM-EDS analysis showed that the RRQG@CDC samples are compact and condensed before adsorbing dyes (Fig. 8A). Additionally, the contents of C (79.14%, from element C of the material skeleton), N (8.93%, from the quaternary ammonium cation -N^+ of the material structure), and Cl (9.23%, from the quaternary ammonium anion Cl^- of the material structure) are high. However, the O content (2.70%, from the residual -OH in the material) was less (Fig. 8B), which indicates that the RRQG@CDC is a type of high-carbon material system with a quaternary ammonium cation structure. After the dyes were adsorbed, the dried RRQG@CDC waste residues showed a more dispersed fragmented particle form (Fig. 8C), while the wet RRQG@CDC waste residues were decomposed into a more dispersed fragment form in water compared to the previous Fig. 7J. This confirms that the RRQG@CDC could adsorb the dyes in water in a highly dispersed form. After dye adsorption, the content of C in the RRQG@CDC waste residues decreased to 65.62%, while the content of N and O increased to 12.34% and 17.36%, respectively. The content of S increased by 3.28% (Fig. 8D). These variations in element concentrations may be due to the doping effect of adsorbed dye elements in the waste residue system. In particular, after the dyes were adsorbed, the content of Cl was significantly reduced to 1.40% (Fig. 8D), indicating that when the RRQG@CDC adsorbs the dyes, sufficient ion exchange takes place and the Cl^- ions in the adsorbent system are replaced, resulting in a significant reduction in the Cl content.

The XRD analysis in Fig. 8E shows the changes in the interior aggregation structures before and after RRQG@CDC adsorbed dyes. Similar to the previous RRQG, before adsorbing dyes, there were a series of sharp peaks at 16.36°, 21.79°, 23.96°, 27.29°, 31.77°, and 45.65° (Curve "a" in Fig. 8E). These indicate that the RRQG@CDC also contains crystalline structures. However, after adsorbing dyes, there was only a wide peak displayed in the XRD curve, which corresponds to an amorphous aggregation structure (Curve "b" in Fig. 8E). This could be because the dyes had been fully adsorbed into the RRQG@CDC structures and the subsequent doping effects caused by this adsorption disrupt the crystal structures of the RRQG@CDC.

The zeta potential analysis in Fig. 8F shows that before dye adsorption, the RRQG@CDC displayed a stronger positively-charged zeta potential of +27.59 eV compared to that of the previous RRQG (+23.17 eV) and a three-dimensional distribution of cation points in a polycationic gel (PPG, +25.55 eV, as reported in one of the authors' previous contributions[25]). This result indicates that the loading interaction of the RRQG with CDC (to form RRQG@CDC) improved the positive polarity of the obtained product. After adsorbing dyes, the zeta potential of RRQG@CDC waste was −14.44 eV, which was very close to that of the previous RRQG (−14.90 eV). The zeta potential of the RRQG@CDC waste was positive (+21.96 eV), possibly because the efficiency of electrostatic interactions had not been fully utilized in the three-dimensional distribution in cation points of PPG. On the whole, the difference in zeta potential of the RRQG@CDC before and after

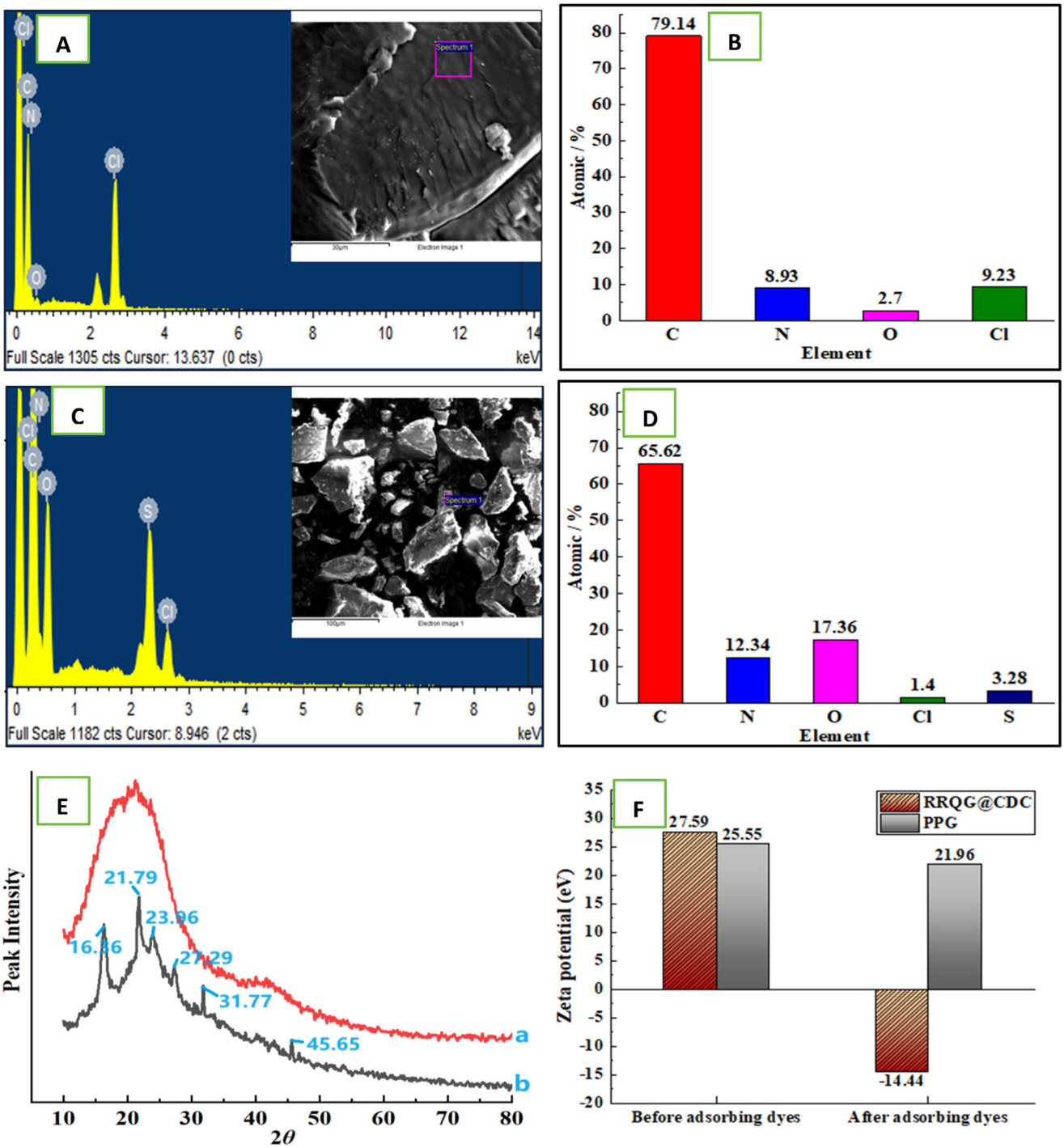

Fig. 8 | SEM-EDS analysis, XRD analysis, and zeta potential analysis comparisons of RRQG@CDC before and after adsorbing dyes. **A** SEM-EDS analysis of RRQG@CDC sample before adsorbing dyes. **B** Element content parameters from the EDS analysis of RRQG@CDC sample before adsorbing dyes. **C** SEM-EDS analysis of RRQG@CDC sample after adsorbing dyes. **D** Element content parameters from the EDS analysis of RRQG@CDC sample after adsorbing dyes. **E** Comparing the XRD analysis of RRQG@CDC before and after adsorbing dyes. **F** Comparing the zeta potentials of RRQG@CDC before and after adsorbing dyes (tested under pH value being 7).

adsorbing dyes was greater than those of the RRQG and PPG, indicating that the adsorption ability of RRQG@CDC towards dyes was stronger than both the RRQG and PPG.

Finally, through XPS, a comparison has been made between the variation in binding energies and key element contents before and after the RRQG@CDC adsorbed dyes. The results are shown in Supplementary Fig. 6 in "Supplementary Information" and the corresponding parameters are listed in Supplementary Table 8. The RRQG@CDC shows three valence bond energy peaks of element N1s at 399.08, 396.67, and 395.62 eV after dye adsorption, while it only has one valence bond energy peak of element N1s before dye adsorption. This may be because the electrostatic interaction between the quaternary ammonium cation, $-N^+$, and dyes in the RRQG@CDC caused the binding energy of the N1s element to shift. Alternatively, the adsorbed dyes were also doped with element N1s which has a new binding energy state. In terms of element contents, the contents of C and Cl in the residue of the RRQG@CDC clearly decreased, while the O

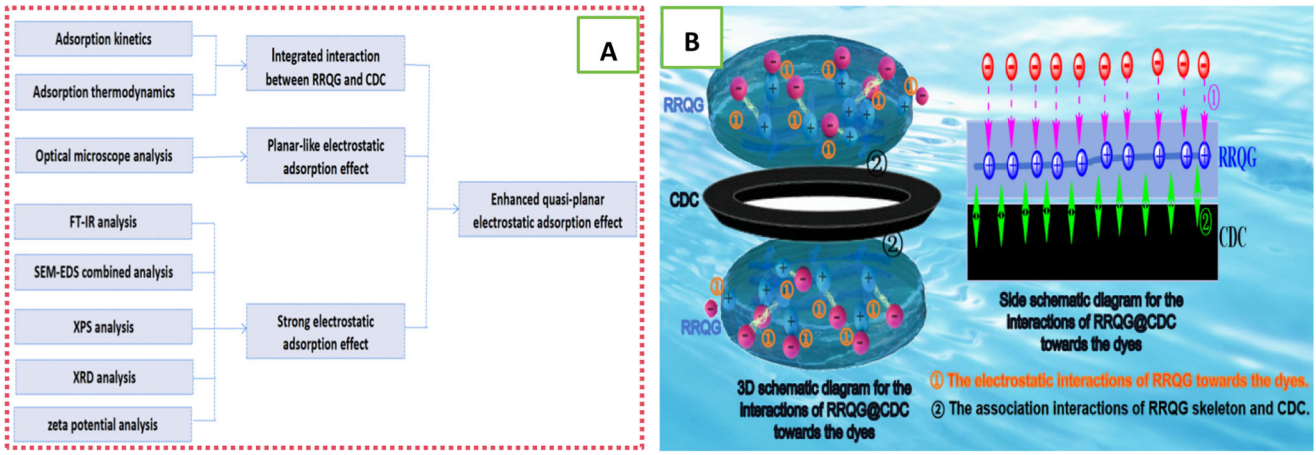

Fig. 9 | Studies on the interaction mechanisms of RRQG@CDC treatment towards dyes. A Logic derivation diagram of the effect mechanism for RRQG@CDC treatment towards dyes. **B** Interaction model diagram of the effect mechanism for RRQG@CDC treatment towards dyes in water.

content clearly increased, which is essentially consistent with the trends shown by the EDS analysis. Furthermore, this once again proved that there is an efficient electrostatic adsorption between RRQG@CDC and the dyes.

By summarizing the experimental results of the studied adsorption mechanisms, a reasonable logical explanation for the adsorption interaction mechanism of the RRQG@CDC towards dyes could be deduced, as shown in Fig. 9A. In this case, the adsorption kinetics and thermodynamic experiments confirmed an integrated interaction occurring between the RRQG and CDC in the RRQG@CDC system. Moreover, the planar-like transition form (e.g., the annular distribution form) and the flake final form after the RRQG@CDC adsorbed dyes were directly observed by optical microscopy, suggesting a planar-like adsorption behavior occurring during the adsorption of dyes by the RRQG@CDC. In addition, several analysis techniques (e.g., FT-IR, SEM-EDS, XPS, XRD, and zeta potential analysis) further confirmed a strong electrostatic adsorption effect occurring in the RRQG@CDC adsorption towards dyes.

In summary, after the logical deduction of an interaction mechanism, it could be confirmed that the RRQG@CDC follows an enhanced quasi-planar electrostatic adsorption mechanism, as shown in Fig. 9B. In the RRQG@CDC material system, the RRQG (as a matrix) produces a quasi-planar electrostatic adsorption based on a flat distribution of the cation adsorption points, leading to the efficient capture of anionic dyes in water [shown as Term ① in Fig. 9B]. At the same time, CDC (as a flat-distributed hydrophobic carrier) produces a face-to-face association interaction with the flat-distributed hydrophobic aliphatic skeleton of the RRQG, promoting the highly directional exposure of hydrophilic cationic adsorption points of the RRQG in water. This could then consolidate the flat distribution of the RRQG cation adsorption points and enhance the quasi-planar electrostatic adsorption [shown as Term ② in Fig. 9B]. Therefore, the RRQG@CDC demonstrates super-efficient adsorption towards dyes in water. This has expanded on the traditional understanding of the adsorption mechanisms in the general three-dimensional adsorbent skeleton spaces.

Resource utilization of waste residues after dye absorption by the RRQG@CDC

Based on thermogravimetric analysis technology, the functional characteristics of waste residues converted into carbonized materials and high calorific fuels after dye absorption by the RRQG@CDC were studied. The aim of this is to utilize solid waste and prevent its subsequent pollution. The results are shown in Fig. 10.

After adsorbing Reactive Scarlet 3BS dye, the RRQG@CDC waste residues became reddish brown (Fig. 10A), while the pure RRQG@CDC samples without adsorption of those dyes were black (see the previous Fig. 4E). This may be the result of an enormous number of colored (red) dyes of Reactive Scarlet 3BS that were enriched in the RRQG@CDC system.

The thermogravimetric analysis results of the RRQG@CDC waste residues in a N_2 atmosphere are shown in Fig. 10B, to investigate the feasibility of converting the waste residues into carbonized materials. The results showed that the first stage weightlessness terminal temperature (T_1) of the RRQG@CDC waste residues samples was 128.6 °C, which is possibly related to the evaporation of inherent moisture. The residual mass percentage was approximately 92.54%. Subsequently, two stages of mass loss occurred continuously, namely the second stage of mass loss (terminal temperature T_2 is 324.41 °C) and the third stage of mass loss (terminal temperature T_3 is 453.55 °C), which may be related to the removal of impurity elements such as N, S, and O in the waste residues. The mass residual percentage was approximately 38.08% and the waste residues formed carbides. Following this, with the continuous increase in temperature, the carbide waste residues slowly degraded and when the upper temperature limit of 900 °C was achieved, its residual mass percentage was only 7.48%, indicating that the carbides which had formed were not stable. This presents a technical limitation in the conversion of the RRQG@CDC waste residues into carbonized materials.

Based on the thermogravimetric analysis results of waste residues in an air atmosphere (Fig. 10C) and according to the parameter analysis method in the "Methods: Analysis of functional characteristics for the resource-based utilization of waste residues" section, it is determined that the ignition and burnout temperatures of waste residues after dye adsorption by the RRQG@CDC are 341.95 and 601.9 °C, respectively. Both of these values are low and the final residual mass ratio of waste residues in an air atmosphere is only 1.85%. From these results, the comprehensive combustion characteristic index is calculated to be 6.169×10^{-10} via Supplementary Equation 10 in "Supplementary Information," indicating that waste residues are easy to burn.

Although the incineration of organic solid waste would produce some carbon dioxide, it could reduce the production of various greenhouse gases, such as methane and carbon dioxide, by replacing landfill disposal methods. Furthermore, incineration could convert organic solid waste into highly calorific energy to replace fossil fuels[39]. Therefore, incineration of organic solid waste can lead to the dual effects of a reduction in emissions and excellent resource utilization.

To sum up, it is feasible to convert the RRQG@CDC waste residues after dye adsorption into high calorific fuels, which could provide a new and effective method for a resource-based treatment of organic solid wastes.

Methods

Materials

DMDAC: 65% (w/w) aqueous solution, Shandong Luyue chemical Group Co., Ltd.; ammonium persulfate (APS): Chemical Book (Shanghai) Initiator Co., Ltd.; hydrochloric acid (HCl): Chengdu Chron Chemical Co., Ltd.; γ-

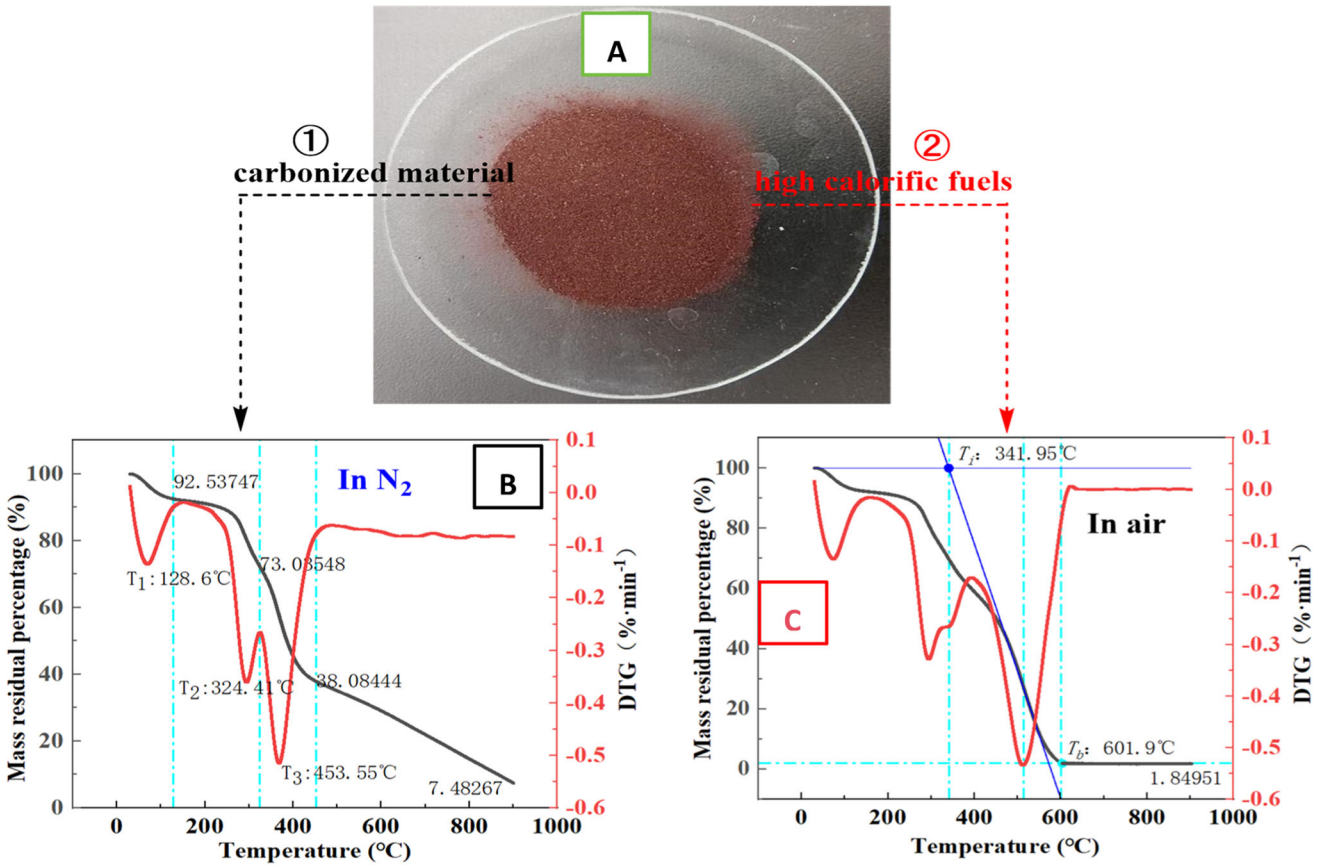

Fig. 10 | Resource utilization of RRQG@CDC waste residues after adsorbing dyes. The practical photo of RRQG@CDC waste residues after adsorbing dyes. **B** TG-DTG analysis of RRQG@CDC waste residues in N_2 atmosphere. **C** TG-DTG analysis of RRQG@CDC waste residues in air atmosphere.

cyclodextrin (γ-CD):Shanghai Macklin Biochemical Technology Co., Ltd.; DHAC: prepared according to the established synthesis method in the previous work of our research group[38]. Diallylamine and epichlorohydrin are used as the main raw materials, which are condensed at room temperature for 4 h and then cyclized at 80 °C for 2 h to obtain DHAC.

Synthesis of RRQG matrix

Firstly, the monomer aqueous solution with a mass fraction of 55% was prepared by mixing the active nitrogen heterocyclic monomer (DHAC) and the comonomer (DMDAC) in a molar ratio of 10:90. Following this, ammonium persulfate (APS) initiator accounting for 3% (w/w) of the monomer mass was added to form a reaction solution.

Then, the reaction solution was heated to 60 °C and for 5 h to obtain a colloid intermediate product. The intrinsic viscosity of the colloid intermediate product was measured as 0.58 dL g^{-1} using the one-point method in a 1 mol L^{-1} NaCl solution at 30 ± 1 °C[23], indicating a polymer formed through the reaction of DHAC and DMDAC. This polymer is herein known as the DHAC-DMDAC prepolymer.

Finally, the DHAC-DMDAC prepolymer colloid was directly heated to evaporate the water solvent without the addition of any regents. The azetidine of the DHAC unit was subsequently opened to be self-crosslinked in situ, thus forming the insoluble RRQG matrix material. The RRQG material was then washed with deionized water three times (liquor ratio of 1:20) to remove unreacted species and dried at 100 °C to obtain the solid products, which are reserved for later use.

Preparation for CDC

CDC was obtained by dissolving 5.0 g of γ-cyclodextrin (γ-CD) in hydrochloric acid at a ratio of 1:9 (v/v), followed by evaporation and drying at 100 °C.

Construction of RRQG@CDC

Initially, 2.0 g of the DHAC-DMDAC prepolymer colloid was soaked in 100 mL of 1% (w/w) γ-CD aqueous solution, ensuring thorough mixing of the components. After evaporating and drying at 100 °C, the DHAC-DMDAC prepolymer formed an RRQG precursor in situ in the γ-CD solution, thus obtaining the γ-CD/RRQG complex. Subsequently, the γ-CD/RRQG complex was mixed with 40 mL of hydrochloric acid in a ratio of 1:9 (v/v) and soaked for 2 h, followed by evaporating and drying at 100 °C to obtain the RRQG@CDC adsorbent materials.

Adsorption experiments

To compare the adsorption effect, a series of adsorption experiments (including isothermal adsorption, adsorption kinetics, and adsorption thermodynamics experiments) for the RRQG matrix and the RRQG@CDC were carried out concurrently. The detailed descriptions can be seen in the "Supplementary Methods: Isothermal adsorption experiments, Adsorption kinetics experiments, and Adsorption thermodynamics experiments" sections in "Supplementary Information."

Analysis of functional characteristics for the resource-based utilization of waste residues

Based on thermogravimetric analysis technology[39–41], the functional characteristics of waste residues converted into carbonized material and high calorific value fuels after dye adsorption by the RRQG@CDC were studied. This was carried out to evaluate the application value of waste residue resources, and the detailed descriptions can be seen in the "Supplementary Methods: Functional characteristics analysis of waste residues converted into carbonized materials, and Function characteristics analysis of waste residues converted into high calorific fuels" sections in "Supplementary Information."

Data availability

The authors declare that all data generated or analyzed during this study are included in this paper.

Received: 6 January 2024; Accepted: 11 June 2024;
Published online: 18 June 2024

References

1. Alsbaiee, A. et al. Rapid removal of organic micropollutants from water by a porous β-cyclodextrin polymer. *Nature* **529**, 190–206 (2016).
2. Penserini, L. et al. An integrated human health risk assessment framework for alkylphenols due to drinking water and crops food consumption. *Chemosphere* **325**, 138259 (2023).
3. Dulsat-Masvidal, M., Ciudad, C., Infante, O., Mateo, R. & Lacorte, S. Water pollution threats in important bird and biodiversity areas from Spain. *J. Hazard. Mater.* **448**, 130938 (2023).
4. Amoah, I. D., Kumari, S. & Bux, F. A probabilistic assessment of microbial infection risks due to occupational exposure to wastewater in a conventional activated sludge wastewater treatment plant. *Sci. Total Environ.* **843**, 156849 (2022).
5. Lin, L., Yang, H. & Xu, X. Effects of water pollution on human health and disease heterogeneity: a review. *Front. Environ. Sci.* **10**, 880246 (2022).
6. Chen, Y. et al. Antibacterial polyvinyl alcohol nanofiltration membrane incorporated with $Cu(OH)_2$ nanowires for dye/salt wastewater treatment. *Sci. Total Environ.* **817**, 152897 (2022).
7. Wan, X., Rong, Z., Zhu, K. & Wu, Y. Chitosan-based dual network composite hydrogel for efficient adsorption of methylene blue dye. *Int. J. Biol. Macromol.* **222**, 725–735 (2022).
8. Yuan, Y. et al. Chlorobenzene levels, component distribution, and ambient severity in wastewater from five textile dyeing wastewater treatment plants. *Ecotoxicol. Environ. Saf.* **193**, 110257 (2020).
9. Wang, X., Ma, X. & Song, C. Deep removal of SO_2 from cathode air over polyethylenimine-modified SBA-15 sorbents for fuel cells. *Catal. Today* **371**, 240–246 (2021).
10. Wei, F., Guo, X., Liao, J., Bao, W. & Chang, L. Ultra-deep removal of thiophene in coke oven gas over Y zeolite: Effect of acid modification on adsorption desulfurization. *Fuel Process. Technol.* **213**, 106632 (2021).
11. Epshtein, A., Nir, O., Monat, L. & Gendel, Y. Treatment of acidic wastewater via fluoride ions removal by SiO2 particles followed by phosphate ions recovery using flow-electrode capacitive deionization. *Chem. Eng. J.* **400**, 125892 (2020).
12. Fisher, K. S. & Vreugdenhil, A. J. Adsorption of chromium (VI) using an activated carbon derived from petroleum coke feedstock. *Int. J. Mol. Sci.* **23**, 16172 (2022).
13. Bilal, M. et al. Remediation of different dyes from textile effluent using activated carbon synthesized from Buxus Wallichiana. *Ind. Crop. Prod.* **187**, 115267 (2022).
14. Jia, Q. et al. Construction of polycationic film coated cotton and new inductive effect to remove water-soluble dyes in water. *Mater. Des.* **124**, 1–15 (2017).
15. Zhang, S. et al. Effect of hydroxyl functional groups on SO_2 adsorption by activated carbon. *J. Environ. Chem. Eng.* **10**, 108727 (2022).
16. Borthakur, P. et al. Computational and experimental assessment of pH and specific ions on the solute solvent interactions of clay-biochar composites towards tetracycline adsorption: Implications on wastewater treatment. *J. Environ. Manag.* **283**, 111989 (2021).
17. Yang, S. et al. Toxic chromium treatment induce amino-assisted electrostatic adsorption for the synthesis of highly dispersed chromium catalyst. *J. Hazard. Mater.* **417**, 126155 (2021).
18. Mashkoor, F. & Nasar, A. I. Carbon nanotube-based adsorbents for the removal of dyes from waters: a review. *Environ. Chem. Lett.* **18**, 605–629 (2020).
19. Liu, G. et al. Activated sludge process enabling highly efficient removal of heavy metal in wastewater. *Environ. Sci. Pollut. Res.* **30**, 21132–21143 (2023).
20. Song, C. et al. One-pot synthesis and combined use of modified cotton adsorbent and flocculant for purifying dyeing wastewater. *ACS Sustain. Chem. Eng.* **65**, 6876–688 (2018).
21. Song, C., Li, H. & Yu, Y. Synthesis, microstructure transformations, and long-distance inductive effect of poly (acrylethyltrimethylammonium chloride) cotton with ultrahigh adsorption ability for purifying dyeing wastewater. *Cellulose* **26**, 3987–4004 (2019).
22. Song, C., Yu, Y. & Sang, X. Synthesis and surface gel-adsorption effect of multidimensional cross-linking cationic cotton for enhancing purification of dyeing waste-water. *J. Chem. Technol. Biotechnol.* **94**, 120–127 (2019).
23. Yang, Q., Bai, Y., Hu, M., Li, M. & Yu, Y. Synthesis of a new polyunsaturated cationic crosslinker by a new micro-polycondensation reaction as a critical modifier of polycationic flocculant for purifying dyeing wastewater. *J. Chem. Technol. Biotechnol.* **96**, 3052–3065 (2021).
24. Hu, M., Xie, N., Gao, S., Huang, Y. & Yu, Y. A super-efficient polyquaternium gel that can remove over-10-times masses of lignins from wastewater for resourcefulness. *npj Clean. Water* **6**, 1–14 (2023).
25. Bai, Y., Song, C., Li, H., Yang, Q. & Yu, Y. Facilely synthesized, highly permeable, and efficiently recyclable polycationic gel with cohesive state transformations for purifying dyeing wastewater. *ACS Omega* **5**, 8046–8055 (2020).
26. Missau, J., Bertuol, D. A. & Tanabe, E. H. Highly efficient adsorbent for removal of crystal violet dye from aqueous solution by CaAl/LDH supported on Biochar. *Appl. Clay Sci.* **214**, 106297 (2021).
27. Zolgharnein, J., Feshki, S., Rastgordani, M. & Ravansalar, S. Simultaneous removal of Basic blue and Toluidine blue O dyes by magnetic Fe_3O_4@polydopamine nanoparticle as an efficient adsorbent using derivative spectrophotometric determination and central composite design optimization. *Inorg. Chem. Commun.* **146**, 110203 (2022).
28. Peng, C. et al. Identification of adsorption or degradation mechanism for the removal of different ionic dyes with iron-carbon micro-electrolysis process. *J. Environ. Chem. Eng.* **9**, 105690 (2021).
29. Chen, W. et al. Assessment of a novel aminated magnetic adsorbent with excellent adsorption capacity for dyes and drugs. *J. Environ. Manag.* **293**, 112809 (2021).
30. Rizzo, C., Misia, G., Marullo, S., Billeci, F. D. & Anna, F. Bio-based chitosan and cellulose ionic liquid gels: polymeric soft materials for the desulfurization of fuel. *Green Chem.* **24**, 1318–1334 (2022).
31. Feng, K. et al. Mesoporous ball-milling iron-loaded biochar for enhanced sorption of reactive red: performance and mechanisms. *Environ. Pollut.* **290**, 117992 (2021).
32. Pandey, S., Do, J. Y., Kim, J. & Kang, M. Fast and highly efficient removal of dye from aqueous solution using natural locust bean gum based hydrogels as adsorbent. *Int. J. Mol. Sci.* **143**, 60–75 (2020).
33. Zhang, W. et al. Unraveling the cation adsorption of geopolymer binder: A molecular dynamics study. *Chemosphere* **335**, 139118 (2023).
34. Usman, M. A. & Khan, A. Y. Selective adsorption of anionic dye from wastewater using polyethyleneimine based macroporous sponge: batch and continuous studies. *J. Hazard. Mater.* **428**, 128238 (2022).
35. Sarmah, D. & Karak, N. Double network hydrophobic starch based amphoteric hydrogel as an effective adsorbent for both cationic and anionic dyes. *Carbohyd. Polym.* **242**, 116320 (2020).
36. Liu, J. et al. Cationic Zr-based metal-organic framework via post-synthetic alkylation for selective adsorption and separation of anionic dyes. *Mater. Today Chem.* **24**, 100897 (2022).
37. Liu, W. et al. Fabrication of polyaniline/poly(vinyl alcohol)/montmorillonite hybrid aerogels toward efficient adsorption of organic dye pollutants. *J. Hazard. Mater.* **435**, 129004 (2022).

38. Li, H., Yang, Q., Hu, M., Bai, Y. & Yu, Y. In-situ synthesis and application of novel renewable polycarboxylate gel-alkali composite water-purification material. *Res. Environ. Sci.* **35**, 1221–1232 (2022).
39. Yu, W. et al. Experimental investigation on the co-combustion characteristics of rice husk and coal. *Trans. Chin. Soc. Agric. Eng.* **39**, 203–211 (2023).
40. Ovcacikova, H. et al. Characterization of waste sludge pigment from production of $ZnCl_2$. *Minerals* **11**, 313 (2021).
41. Han, Y. & Li, H. A new, improved method to identify reaction mechanisms based on the shape of derivative thermogravimetric curves. *Case Stud. Therm. Eng.* **45**, 102993 (2023).

Acknowledgements

We acknowledge the financial support provided by the National Nature Science Foundation of China (Project No. 21866016) and the Nature Science Foundation of Jiangxi Province, China (Project No. 20232BAB203034).

Author contributions

Menghan Hu: performed the experiments, data and literature analyses, and wrote the manuscript. Na Xie: assisted the experiments, and data analyses. Yujia Huang: assisted the experiments, and literature analyses. Yikai Yu: contributed to the conception of the study, contributed significantly to analysis and manuscript preparation, helped perform the analysis with constructive discussions, and revised the manuscript.

Competing interests

The authors declare no competing interests.

Additional information

Supplementary information The online version contains supplementary material available at https://doi.org/10.1038/s41545-024-00347-0.

Correspondence and requests for materials should be addressed to Yikai Yu.